CHARACTERIZATION OF TRANSONIC BUFFET ON A SWEPT WING BY MEANS OF CRYOGENIC PIV

C. J. Schauerte*, J. Bosbach†, R. Konrath†, R. Geisler†, F. Philipp†, A.-M. Schreyer*

* RWTH Aachen University, Institute of Aerodynamics and Chair of Fluid Mechanics, Wüllnerstraße 5a, 52062 Aachen, Germany

† German Aerospace Center, Institute of Aerodynamics and Flow Technology, Bunsenstraße 10, 37073 Göttingen, Germany

Abstract

Transonic buffet is one of the major factors in the aerodynamic design of modern transport aircraft. The phenomenon is encountered on the suction side of airfoils in transonic flow. It is associated with low-frequency shock oscillations coupled with a periodic modulation of the large-scale shock-induced flow separation. Buffet can induce detrimental structural vibrations (buffeting) and thus strictly limits the flight envelope. Various aspects of the phenomenon remain not fully understood, in particular where realistic 3D aircraft wings and high, flight-realistic Reynolds numbers are concerned. In the present study, we characterize transonic buffet on a swept wing at a Mach number of Ma=0.84 and a high Reynolds number of Re=12.9 Mio (based on the mean aerodynamic chord), thus fostering a comprehensive understanding of 3D buffet near the limits of the flight envelope. A full-span model of the XRF1 airplane geometry designed by Airbus was investigated in cryogenic conditions (T_0=180 K) in the European Transonic Wind Tunnel (ETW), Cologne, Germany. An in-depth discussion of the velocity field measured by means of cryogenic Particle Image Velocimetry (cryoPIV) is presented. Two consecutive and spatially linked fields of view on the wing and in its wake allow to capture the flow physics across a large region. The nature of the unsteady flow topology induced by an oscillating shock wave at established buffet conditions is explored in terms of phase-averaged velocity maps. A thorough analysis of the mean and turbulent velocity field is complemented by a statistical evaluation of turbulent quantities. High-speed PIV sequences in the wing wake are explored to capture the spectral signature induced by transonic wing buffet and to assess the fluctuations imposed on the wing wake. Inherent fluctuations continue to exist as they are convected downstream, and maintain a spectral composition typical of 3D buffet. Consequently, buffet severely affects also the downstream flow conditions.

Contact address:

c.schauerte@aia.rwth-aachen.de

1. INTRODUCTION

The transonic flow around airfoils and swept wings is often accompanied by locally supersonic regions on the upper surface that are terminated by a shock wave [1]. Shock-induced flow separation may span the entire region from the shock to the trailing edge [2]. For certain combinations of Mach number, Reynolds number, and angle of attack, the transonic flow past an airfoil or the suction side of transport-type wings can become unsteady [3]. The resulting complex shock-wave/boundary-layer interaction – typically referred to as transonic buffet – involves major parts of the flow field. It is associated with low-frequency shock oscillations that are coupled with a periodic modulation of the large-scale shock-induced flow separation [4].

Immediate consequences of transonic buffet are diverse, since they not only reduce the aerodynamic performance but may also impose severe loads on the airframe [5]. Transonic buffet is, inter alia, associated with a highly unsteady flow field [2], severe oscillations of the lift coefficient [6], and fluctuating aerodynamic forces on the aircraft [5]. While these immediate and unavoidable consequences of buffet, i.e. fluctuations of the integral quantities, are unfavorable in themselves, the mechanical coupling with the airframe is even more severe. It can lead to a detrimental structural response (buffeting), which may damage the aircraft [6].

Self-sustained unsteady shock-wave motion in the context of transonic flow about airfoils has been first mentioned seven decades ago [7]. Even though many profound experimental and numerical studies [1, 3, 4, 8–10] have been dedicated to the topic since then, a complete understanding of the underlying mechanisms is still lacking [11].

With a growing demand for fast and sustainable air travel, the use of supercritical wings increases, and the overall efficiency of modern civil aircraft becomes increasingly relevant [12]. Several decades of research reveal that transonic buffet is one of the major challenges when it comes to aircraft performance [13]. As buffet onset practically constrains the usable range of the flight envelope [2, 5], a profound understanding of the phenomenon is the prerequisite to shift the limits of the flight envelope and crucial

doi: 10.25967/570369

for the aerodynamic design of modern transport aircraft [14].
For the inherently 3D configurations of wings with finite span and non-zero sweep angles, and in particular for aircraft wings at high, flight-realistic Reynolds numbers, the situation becomes even more complex than for 2D airfoil configurations.
The root causes of the observed intense pressure fluctuations, i.e. shock oscillations and flow separation were similarly identified both for the buffet regime on 2D airfoils and for high-aspect ratio, transport-type, swept wings in transonic flow [15]. In spite of qualitative similarities, several unique features are specifically observed for swept wing configurations [16]. Substantial differences in the exact nature and global organization of airfoil and swept-wing buffet were also reported in subsequent studies [2, 17, 18], amongst them a significant contribution of convection velocities and the propagation of pressure information in the spanwise direction. These findings suggest that different mechanisms are governing.
3D buffet cells form and convect in the spanwise direction along the swept wing, generating a complex and intricate three-dimensional flow field. At fully-developed buffet conditions, the most severe large-scale unsteadiness is concentrated around the outboard region [11]. For particular operating conditions an aperiodic character of the intense broadband shock motion localized around the wingtip section was identified [19]. Also the characteristic decay of the shock oscillation beyond conditions of pronounced buffet observed in 2D configurations [1, 20], referred to as buffet offset, could not be reproduced in 3D configurations [17, 18].
Characteristic frequencies of the periodic shock oscillation are 4-7 times higher for swept wings than for 2D cases [21], whereas the shock amplitudes are much larger on 2D airfoils. In addition, the spectral properties of the shock motion are broadband in nature for swept wings [5], i.e. the energy contribution of the oscillatory shock motion is spread across a broader frequency range, whereas a distinct peak is commonly observed for airfoil buffet [4]. Related Strouhal numbers based on chord length also differ: 0.2-0.6 is observed for swept-wing buffet [11], and only about 0.05-0.07 for purely 2D cases [18]. Consequently, capturing 3D buffet by just a few parameters is challenging.
Despite the elusive nature of 3D buffet, Paladini et al. [18] recently identified several key parameters that remain constant among different investigations and thus allow to directly compare findings from different studies. Dimensionless numbers, such as the Strouhal number and the dimensionless convection velocity, are amongst these parameters.
Even less attention than to wing buffet itself has been paid to the impact of buffet-induced modifications of the wake so far. Due to the extent of the flow variations for fully-developed buffet conditions, such perturbations are expected to persist in the wake, convect downstream, and potentially affect control surfaces impacted by the wake, such as the tailplane.
Embedded into the DFG research unit FOR 2895, our present study aims at fostering a comprehensive understanding of 3D buffet, including its influence on the wake flow, near the limits of the flight envelope. For that purpose, we characterize transonic buffet on a swept wing at a Mach number of Ma=0.84 and a Reynolds number based on the mean aerodynamic chord of $Re = 12.9 \cdot 10^6$. A full-span model of the XRF1 airplane geometry designed by Airbus was investigated in cryogenic conditions in the European Transonic Wind Tunnel (ETW), Cologne, Germany. The experimental setup and methods are presented in Sec. 2, and we provide an in-depth discussion of the flow topology around the wing throughout the buffet cycle, as well as the velocity field measured by means of cryogenic Particle Image Velocimetry (Sec. 3). We then discuss the influence of buffet on the wake flow in Sec. 4 and present our main conclusions in Sec. 5.

2. EXPERIMENTAL SETUP

In this section, we provide an overview of the wind tunnel facility, the investigated aircraft model, as well as the applied experimental methods.

2.1. European Transonic Windtunnel

All experiments were conducted in the cryogenic wind tunnel facility European Transonic Windtunnel (ETW) located in Cologne, Germany. ETW is a continuously operated wind tunnel with a closed aerodynamic circuit. The test section with a height of 2 m and a width of 2.4 m is encapsulated in an insulated stainless steel pressure shell with a diameter of about 10 m designed for cryogenic operating conditions. The facility can accommodate both semi-span and full-span models.
The concept of a pressurized test chamber and an independently adjustable temperature regime allows to control and set the desired key parameters (Mach number, Reynolds number, and dynamic pressure) independently. The ETW can thus accurately simulate realistic high-lift and high-speed flight conditions of modern transport aircraft. To achieve the desired low temperature in the test section, liquid nitrogen with a temperature of -196 degrees Celsius is continuously injected into the tunnel flow upstream of the compressor. This liquid nitrogen vaporizes immediately and forms a cold gas flow with total temperatures down to 110 K and total pressures of up to 450 kPa. The compressor with a maximum drive power of up to 50 MW circulates the nitrogen test gas around the circuit.

2.2. Wind-tunnel model

A wind-tunnel model of the XRF1 aircraft geometry was explored in this study. The full-span sting-mounted model was developed and provided for the present test campaign by Airbus. It was particularly designed for cryogenic test environments and manufactured from stainless steel. The total span

is 1.56 m and the mean aerodynamic chord (MAC) is 0.1965 m. Both the pressure and suction sides of the wing are equipped with unsteady pressure transducers to capture unsteady loads associated with buffet operating conditions.

2.3. CryoPIV measurement arrangement

We intended to analyze both wing buffet in the direct vicinity of the shock wave and the wake of the wing in detail. The measurement layout depicted in Fig. 1 enables us to capture both regions of interest. Two consecutive fields of view cover the flow on the wing and in its wake, with an overlap to link both regions.
In both fields of view, we measured velocity fields using the cryoPIV-technique developed by DLR for application in the cryogenic test environment of ETW. We employed a combined setup consisting of a) a low-speed PIV approach focused on the wing suction side (being a more sophisticated future stage of the one introduced in [22]) and b) a high-speed PIV system capturing the wake region, being an advanced version of the one described in [23]. The stereoscopic measurement arrangement in both domains provides access to all three velocity components in the field of view.
Several flush-mounted windows in the side, top, and bottom walls of the ETW test section provide optical access. The cameras and light sheet optics are mounted outside of the test chamber, but still within the cryogic environment. Therefore, all optical modules are installed in heated housings. Once the cooling-down procedure of the facility is initiated, access to the pre-conditioned and pressurized test section is precluded. All optical modules (including the light sheet-forming optics and electronics) are integrated in a fully remote-controlled measurement setup, which allows to re-adjust all components to compensate for temperature-dependent deviations of the optical paths.
Tracer particles consisting of tiny ice crystals were generated from a water aerosol injected into a cryogenic chamber and added to the flow. This seeding material was chosen to prevent any damage to the insulation material of the wind tunnel. Any residual particles evaporate completely when warming-up the wind tunnel circuit after completing the test campaign. This approach ensures a residue-free seeding while meeting the requirements for accurate and reliable PIV measurements, including a decent signal to noise ratio and small-enough particles to control particle slip and thus the measurement uncertainty.
Acquisition of the low-speed PIV system on the wing suction side is based on a fast double shutter triple-frame approach as introduced by Geisler [24]. Particles on the wing upper side were illuminated by two identical Innolas SpitLight 1000 dual cavity Nd:YAG lasers with a repetition rate of 10 Hz. The laser system provides short pulses with a pulse duration of 6 ns and an energy of 130 mJ per pulse. Recording of the obtained particle images was based on the FOX technique [24] using CCD-based image sensors with a spatial resolution of 2048 x 2048 pixels. The covered field of view was 140 mm wide and 85 mm high. Particle images of the wake region are captured using two identical Phantom v2640 high-speed cameras with a resolution of 4 megapixels, which corresponds to a sensor resolution of 2,048 pixels x 1,952 pixels. The captured domain in the measurement plane is 160 mm wide and 170 mm high. Particles in the measurment plane are illuminated by a Photonics DM200-532 dual cavity Nd:YAG high-speed laser with an energy of 27 mJ per pulse and a pulse width of 180 ns. The resulting temporal resolution of the vector fields is 3.3 kHz. The light sheet thickness across the captured domain of both systems was kept constant at 1-2 mm. The resulting combined field of view of both systems spans a domain from $x/c \approx 0.3$ to $x/c \approx 1.9$. The measured data enable us to capture the flow physics, which we studied on the basis of a thorough analysis of the mean and turbulent velocity field, its variation associated with the buffet condition, as well as of the spectral content of the turbulent wing wake.
Further details on the setups and alignment procedures of cryoPIV in ETW will be provided elsewhere.

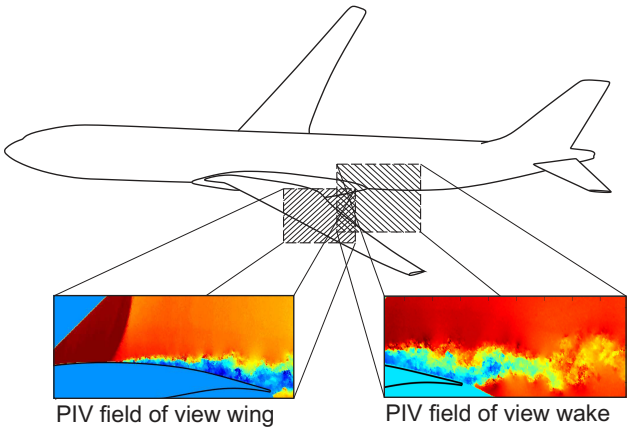

FIG 1. Schematic representation of the measurement arrangement on a generic aircraft configuration and exemplary velocity fields obtained from PIV measurements of a 2D buffet case (shown here for illustration)

3. RESULTS FOR SWEPT-WING BUFFET

In the subsequent sections, we discuss results from CryoPIV measurements and characterize the topology and turbulence behavior for swept-wing buffet. First, we present and discuss the global flow conditions that characterize the studied buffet condition.

3.1. Characterization of the buffet cycle

We performed a detailed assessment of the variation of the flow topology to quantify the shock-induced unsteadiness and the severity of the shock oscillation associated with the present buffet condition. Since the flow field varies strongly, we compute multiple

phase-averaged representations throughout a cycle. To do so, instantaneous velocity fields from PIV were classified with respect to the chordwise shock location. This was found to be a reliable indicator to resolve the shock motion and the large-scale modifications of the flow field modulated by the shock motion. We extracted the shock line from 12,500 snapshots at 5 vertical stations above the wing. An equivalent approach was used in [25] to describe fully-established airfoil buffet.

For this swept wing configuration, we expected a substantially reduced shock amplitude compared with the 2D case [18]. An evaluation of the most upstream and downstream shock locations indicate a maximum shock amplitude of $0.05\,c$ (expressed in chord percentages). In addition, no significant distinction between phases of shock upstream or downstream movement could be identified. Based on these observations, we chose three characteristic phases, defined by the shock most upstream, most downstream, and a central position, for further analysis. Fig. 2 shows the ensemble-averaged streamwise velocity u contours (normalized with the velocity u_∞ of the incoming flow) for the above defined phases superimposed with the corresponding velocity contours at discrete chordwise stations $x/c = 0.4$, $x/c = 0.6$, $x/c = 0.8$, $x/c = 1.0$, and $x/c = 1.2$.

The three presented phase-averaged velocity maps capture the large-scale organization of the flow. A supersonic region on the wing suction side is terminated by a shock wave located between $x/c = 0.40$ and $x/c = 0.45$, depending on the phase. The massive drop in streamwise velocity across the shock is clearly visible in the velocity profiles downstream. The shock wave causes the boundary layer downstream to thicken and finally separate when approaching the trailing edge. This behavior is indicated by the pronounced low-speed region developing around $x/c \approx 0.85$ in all phases (see Fig. 2 (a) - (c)). The pronounced flow separation is also reflected in the velocity deficit observed at $x/c = 1.0$, which persists until the near-wake ($x/c = 1.2$).

These global properties persist throughout all phases of the buffet mode (see Fig. 2 (a)-(c)). However, three aspects allow to distinguish the phases and are characteristic for the variation within the cycle. First, the chordwise shock location moves from about $x/c = 0.40$ to $x/c = 0.45$ between the shock's most upstream and downstream positions. The thus extracted amplitude of the shock displacement ($A_s = 0.05\,c$) is about one order of magnitude lower than for 2D buffet [4], which is in perfect agreement with findings from the literature [18]. Second, due to the curvature of the shock wave, the velocity profile at $x/c = 0.60$ intersects the shock transition region. Therefore, when the shock wave is farthest upstream (see Fig. 2 (a)), the entire velocity profile is in the post-shock domain. For the phase with the farthest downstream shock location on the other hand, the velocity profile protrudes into the pre-shock domain, and the higher upstream velocity values are reached

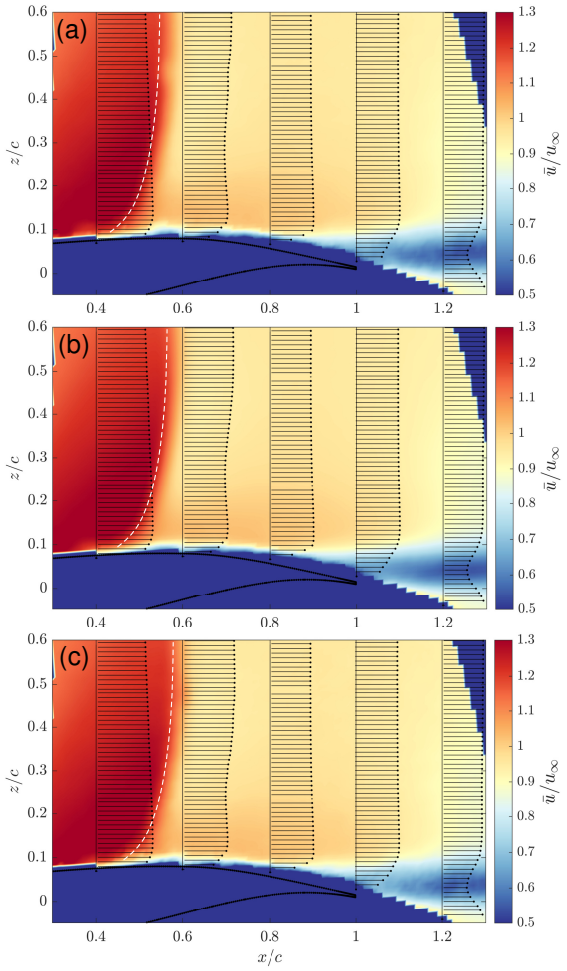

FIG 2. Phase-averaged streamwise velocity component for three chordwise shock locations: most upstream (a), central (b), and most downstream (c); airfoil not to scale

for $z/c = 0.3$ (see Fig. 2 (c)). Third, the velocity deficit at $x/c = 1$ and $x/c = 1.2$ is largest for the most upstream shock location.

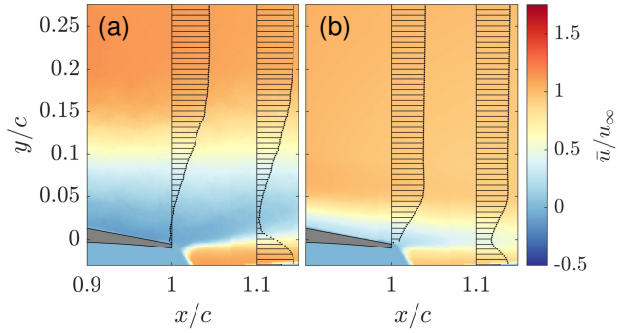

FIG 3. Phase-averaged streamwise velocity component for the different chordwise shock locations, most upstream (a) and most downstream (b) for fully-established 2D buffet [25]

The latter aspect is qualitatively similar for 2D buffet on an airfoil, although the absolute variation is substantially smaller than for an airfoil, both in terms of the shock excursion and the resulting modification to

the flow field. This difference is clearly visible when comparing Figs. 2(a) and (c) with Fig. 3, which shows the velocity maps for the most upstream (a) and most downstream (b) shock locations of a fully-developed buffet on a supercritical airfoil [25]. For the 2D case, the global variation of the flow field throughout the buffet cycle is much more severe, which is clearly visible in the velocity contours: in the upstream phase (Fig. 3(a)), the separation is much larger and persists until the trailing edge.
In the presently studied swept wing case, the separation and velocity deficit a) are much smaller and b) vary much less over the buffet cycle: the velocity profiles at $x/c = 1.0$ and $x/c = 1.2$ for all phases of the shock motion resemble the state of a far-downstream shock wave in the airfoil case (Fig. 3 (b)).
The small changes in global flow topology are most probably related to the spatially limited excursion of the shock wave and the reduced distinctness in shock-motion periodicity associated with wing buffet [26] (as compared with a strictly periodic, quasi-sinusoidal behavior in 2D airfoil buffet [4, 25]).
Interestingly, the variation of the shock location is not linked with a strongly varying nature of the shock shape and obliqueness. This observation follows from an almost constant curvature of the shock line and thus a virtually invariant shock strength, which further contributes to the less pronounced variation of the overall flow field.
Due to the small observed variations of the flow field, we calculate all subsequent statistics from an ensemble-averaged representation instead of the phase averages shown so far.

3.2. Global flow topology and mean velocity field on the wing suction side

In the previous section, the buffet condition was discussed in terms of the involved variation associated with the oscillatory up- and downstream motion of the shock. Furthermore, we discussed the streamwise velocity component. In this section, we focus on the development of the flow along the two remaining directions of motion in the captured measurement plane. We thus provide a detailed description of the global organization of the flow past this swept wing configuration based on the measured velocity fields.

3.2.1. Wall-normal velocity component

To complement the streamwise velocity maps and corresponding profiles discussed in section 3.1, we provide details on the vertical velocity component in this paragraph.
The streamwise velocity component (Fig. 2) reveals a considerable re-distribution of momentum caused by the shock wave. This redistribution is noticeable in the reduced fullness of the streamwise velocity profiles downstream of the shock and in a substantial velocity deficit emerging upstream of the trailing edge.
As the shock wave is distinctly oblique with respect to the wing surface in the near-wall region, we expect a non-zero shift in the wall-normal velocity component (w). Fig. 4 shows the ensemble-averaged vertical velocity contour along with profiles at the same chordwise stations as in Fig. 2. The maximum magnitude of the wall-normal velocity is on the order of $w_{peak} \approx 0.2 \cdot u_\infty$. In the supersonic region upstream of the shock wave (velocity profile at $x/c = 0.4$), positive values of w denote an upwards deflection of the flow. This upwards component increases steadily with growing distance from the wing surface. Upon traversing the shock plane, both the contour and the profile at $x/c = 0.6$ reveal a strong upwards deflection ($\overline{w} \approx 0.12\, u_\infty$) that remains at a constantly high level up to $z/c \approx 0.3$. This region coincides with the greatest detected value w_{peak}.

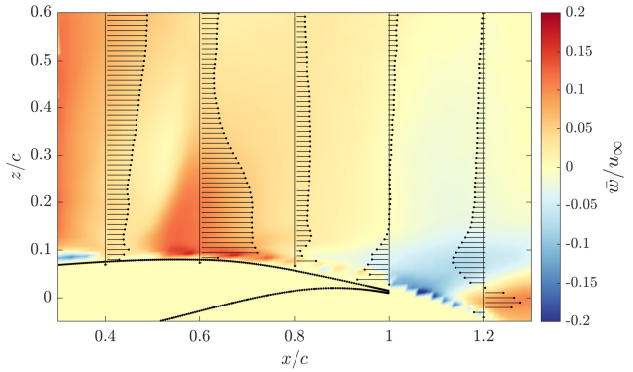

FIG 4. Ensemble averaged vertical velocity contour (airfoil not to scale)

Farther away from the surface, the wall-normal velocity component decreases strongly since the shock becomes exactly vertical for $z/c \geq 0.4$ (see Fig. 2), such that neither additional upwards nor downwards deflection is induced. This effect is intensified by a gradual downwash when the flow follows the curvature towards the aft part of the wing. These effects are visible across the velocity profiles at a vertical station $z/c = 0.5$ and are used as an indicator of the evolution of the vertical momentum distribution: The positive value of $w/u_\infty = 0.05$ at $x/c = 0.4$, indicates an upwards deflection whereas at the same vertical location of $z/c = 0.5$, the velocity becomes slightly negavtive ($w/u_\infty = -0.025$) at $x/c = 1.2$, which indicates a slight downwards component.

3.2.2. Spanwise velocity component

Since communication in the spanwise direction is one of the predominant mechanisms that differentiate transonic buffet on swept wings from 2D buffet on airfoils [27], we discuss the spanwise velocity component (shown in Fig. 5) here.
Both in-plane velocity components indicated that the shock wave dissipates a significant portion of the kinetic energy and also re-distributes the momentum downstream of the shock.
In the spanwise component, the induced modification is not as severe as for the vertical velocity, however, the momentum distribution seems to change continu-

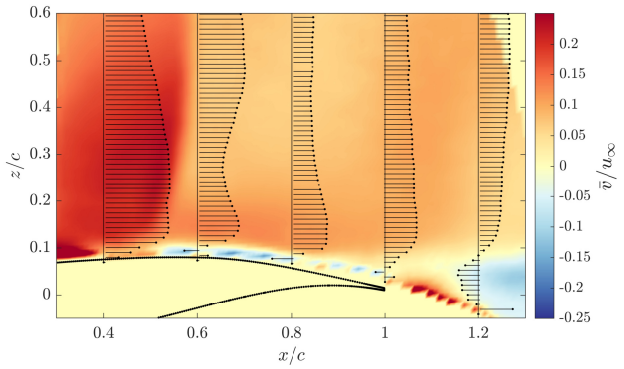

FIG 5. Ensemble averaged spanwise velocity contour (airfoil not to scale)

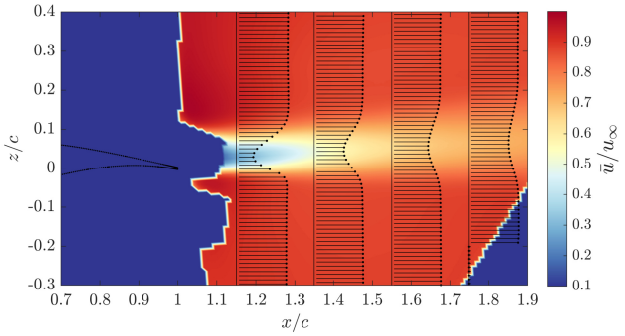

FIG 6. Ensemble averaged streamwise velocity contour in the wake region (airfoil not to scale)

ously along the wing surface. Therefore, each chordwise station exhibits a unique velocity profile. A peak velocity value of $v_{peak} \approx 0.25 \cdot u_\infty$ is detected in the supersonic region slightly ahead of the shock front at a height $z/c \approx 0.3$ (see Fig. 5). The profile at $x/c = 0.6$, immediately downstream of the shock wave, is characterized by a pronounced velocity deficit ($v \approx 0.08u_\infty$) at $z/c \approx 0.25$, which is framed by regions of greater velocities. At $x/c = 0.8$, the spanwise component is strongly reduced for $z/c \geq 0.35$ compared with both the pre-shock and the post-shock locations at $x/c = 0.4$ and $x/c = 0.6$, respectively. The spanwise velocity component increases again towards the aft section of the wing ($x/c \geq 0.9$), and a very even distribution of the spanwise velocity with a value of about $0.5 \cdot v_{peak}$ is obtained at the trailing edge location. Note that the spanwise velocity is consistently positive all along the wing suction side.

4. VELOCITY FIELD IN THE WAKE OF THE WING

The following discussion is dedicated to the wake of the wing. We aim at acquiring a better understanding of the buffet-induced disturbances propagating downstream. First, we discuss ensemble-averaged velocity contours and profiles, then we assess the turbulent perturbations. The section is concluded with an examination of the spectral content of the wake flow.

4.1. Ensemble-averaged velocity maps

Contours of the mean streamwise velocity component are shown in Fig. 6. As expected from our observations in the near-wake region between $x/c = 0.8$ to $x/c = 1.0$ (see Fig. 2), the streamwise velocity profiles are only considerably affected by the wake of the wing in a narrow range around the centerline. The greatest velocity deficit is observed in the immediate vicinity of the trailing edge at $x/c = 1.15$. The lowest value of $\overline{u}_{min} = 0.3 \cdot u_\infty$ is reached in the horizontal extension slightly above the trailing edge. As stated earlier, this level of deficit is comparable with phases of less severe separation in fully-established airfoil buffet.

The streamwise velocity recovers fast, and regains minimum values of $\overline{u}_{min} = 0.6 \cdot u_\infty$ and $\overline{u}_{min} = 0.8 \cdot u_\infty$ at only $0.25\,c$ and $0.75\,c$ downstream of the trailing edge, respectively. Simultaneously, the profiles flatten out with a growing vertical extent that increases from $\Delta z/c = 0.2$ to $\Delta z/c = 0.35$ between the horizontal stations $x/c = 1.15$ and $x/c = 1.75$. The rapid recovery can most likely be attributed to a high level of turbulent mixing associated with the w-component. This aspect will be addressed in more detail in the subsequent section.

The vertical velocity component in the wake is plotted in Fig. 7. The good agreement of the velocity profile at $x/c = 1.15$ with the corresponding location of the wing FOV (Fig. 4) underlines the consistency between the two independent measurements of the consecutive fields of view.

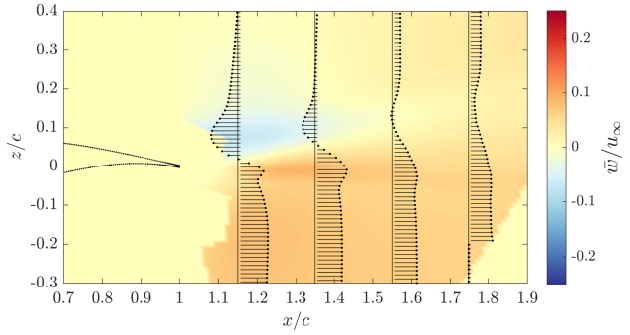

FIG 7. Ensemble averaged vertical velocity contour in the wake region (airfoil not to scale)

Downstream of the trailing edge, the flow fields from the suction and pressure side coalesce and an interaction zone between regions of opposite sign forms. As was seen in Fig. 4, a distinct downwash originates from the aft part of the suction side. This influence persists into the downstream domain and is only overcome by the considerably stronger upwash from the pressure side; beyond $x/c = 1.55$, the vertical velocity is consistently positive.

Regarding the spanwise velocity component, the flow field is bisected by a virtual horizontal line at $z/c \approx 0.1$ (see Fig. 8). Above the wake core, the spanwise velocity is consistently positive, while it is negative in the entire lower half of the flow field.

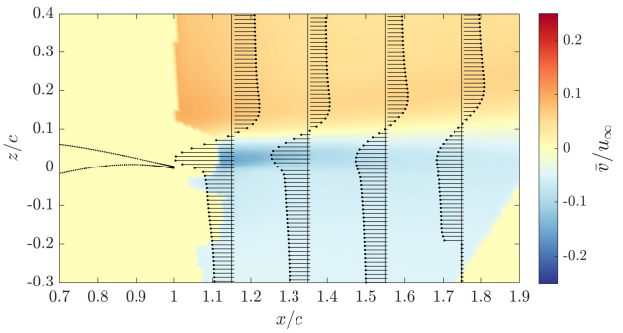

FIG 8. Ensemble averaged spanwise velocity contour in the wake region (airfoil not to scale)

The magnitude of the positive and negative velocities on the suction and pressure sides, respectively, is fully-balanced and almost constant at $\pm 0.2 \cdot u_\infty$ all along the streamwise coordinate; only locally, at the onset of the mixing zone (see velocity profile at $x/c = 1.15$), excess velocities of about $-0.2 \cdot u_\infty$ are observed. This excess amount is gradually dissipated and has disappeared entirely at $x/c = 1.75$.

4.2. Turbulent quantities in the wing wake

In this section, we discuss the turbulent intensities of the streamwise, vertical, and spanwise velocity components. For swept wings, the shock buffet dynamics are assumed to be accompanied by a distinct spanwise contribution, in contrast to 2D airfoil buffet, where a vanishing mean spanwise perturbation is expected [18]. This exchange of information along the wing axis is responsible for the formation and convection of buffet cells that partially explain the more intricate and 3D nature of wing buffet [11, 28].

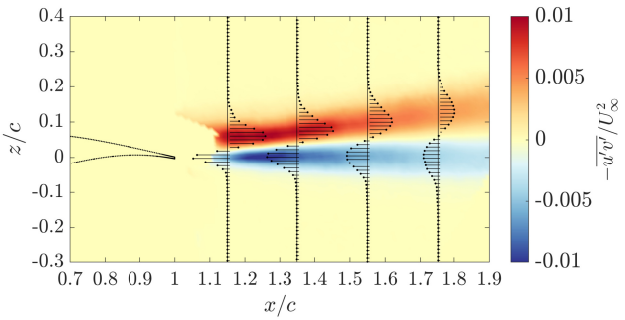

FIG 9. Contour map of the Reynolds shear stress component $-\overline{u'w'}/u_\infty^2$ in the measurement plane (airfoil not to scale)

Fig. 9 provides an overview of the Reynolds shear stress component $-\overline{u'w'}/u_\infty^2$. The contour map shows a characteristic pattern consisting of two distinct streaks of increased shear stress intensities with opposite sign. The streaks diverge slightly from the wake main axis with increasing downstream distance. Peak intensities are observed in the vicinity of the trailing edge at $x/c = 1.15$ and remain at a constantly high level until about $x/c = 1.4$. Farther downstream, the intensity decreases, and the bumps are spread out towards the free stream. The displayed shear stress distribution provides an estimate of the extent of the wake; it indicates a weakly diverging wake with a maximum expansion of $0.3\,c$ at a horizontal distance of $0.9\,c$ from the trailing edge. Outside of the shear-dominated wake region, the profiles converge to zero, as expected for measurements with a low noise level.

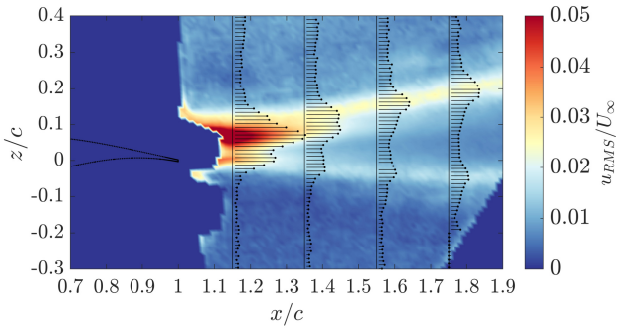

FIG 10. Streamwise velocity fluctuation component u_{RMS}/u_∞ in the wake (airfoil not to scale)

The intensity of the streamwise turbulence component is given Fig. 10 in terms of the values u_{RMS}. From the contour plot, it is apparent that greatest intensities occur in the upper wake flow and are aligned with the upper edge of the wake (which was previously identified in Fig. 9).
The evolution in the streamwise direction is as follows: close to the trailing edge ($x/c = 1.15$), the u_{RMS}-profile has a Gaussian-like shape, where the greatest magnitude is located at the wake core. Farther downstream (until about $x/c = 1.75$), the turbulence intensity decreases in the core area. This region of decreased turbulent mixing is framed by individual intensity bumps on either side, whose distance increases with downstream distance x/c. The maxima thus follow the bounds of the turbulent wake. This behavior results in M-shaped turbulence profiles for $x/c \geq 1.4$, emphasizing an asymmetric nature of the wake flow with greatest fluctuations shifted towards the upper half of the wake.

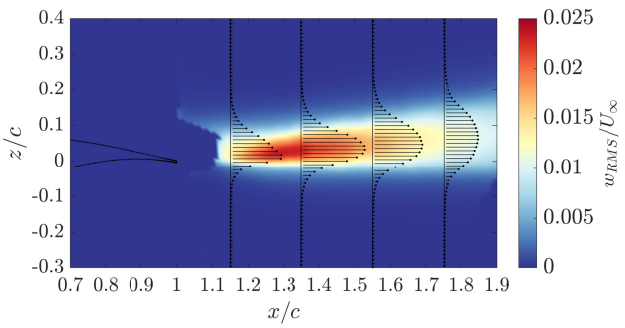

FIG 11. Vertical velocity fluctuation w_{RMS}/u_∞ in the measurement plane (airfoil not to scale)

The behavior of the turbulent fluctuations in the vertical direction strongly differ from the two previously reported quantities $-\overline{u'w'}/u_\infty^2$ and u_{RMS}/u_∞. The turbulence contour in Fig. 11 illustrates that the region of intense vertical fluctuations is spatially confined within

the wake; its maximum value is along the wake main axis, and the intensity sharply declines towards zero at the edges.
The overall magnitude of the vertical turbulence intensity is about twice as large as for the Reynolds shear stress component $-\overline{u'v'}/u_\infty^2$. From the contour map, it can be seen that the wake main axis shifts slightly upwards with downstream development, such that the wake core is centered around $z/c = 0.02$ close to the trailing edge, while it is displaced up to $z/c = 0.08$ at $x/c = 1.8$ (see Fig. 11).
Overall, Fig. 11 emphasizes the great level of turbulent mixing associated with the vertical component. We assume that this mixing is mainly responsible for the rapidly recovering velocity profiles of the u-component (see Fig.6), as it allows for the exchange of high-momentum fluid from the regions below and above the wake.

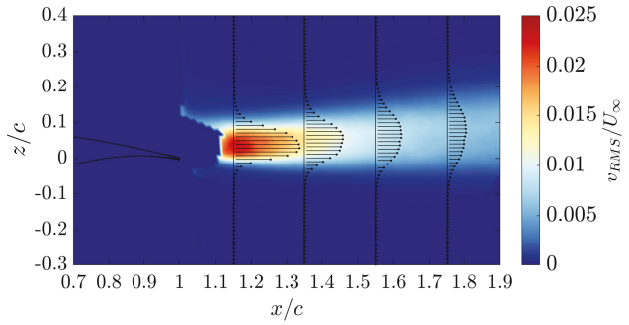

FIG 12. Spanwise velocity fluctuation v_{RMS}/u_∞ in the measurement plane (airfoil not to scale)

Fig. 12 presents the spanwise turbulent intensity in terms of the v_{RMS}/u_∞ component. The spanwise perturbation is greatest slightly downstream of the trailing edge in the flow from the upper surface. The peak intensity is reached earlier (at $x/c = 1.15$) than for the vertical component w_{RMS}/u_∞ (maximum reached at $x/c = 1.35$; see Fig. 11) and declines within a short distance from the trailing edge. This indicates that spanwise perturbations are dominated by the interaction with the trailing edge. Just as the vertical fluctuation component, w_{RMS} values are almost symmetric with respect to the peak contribution centered around the wake main axis at all streamwise locations.

4.3. Spectral analysis of the velocity fluctuations

To capture the spectral signature induced by the shock unsteadiness, we evaluated the high-speed PIV measurements in the wing wake with respect to streamwise velocity fluctuation at discrete stations along the wake core between $x/c = 1.1$ and $x/c = 1.9$. With the recording frequency of 3.3 kHz, spectral content at frequencies associated with the buffet shock motion (which is on the order of $\mathcal{O}(400 - 800)$ Hz can be resolved.
We selected four analysis windows at longitudinal locations $x/c = 1.2$, $x/c = 1.4$, $x/c = 1.6$, and $x/c = 1.8$; these are marked in Fig. 13 (a). For each snapshot of the sequence and each analysis window, the spatial average over a 3 by 3 array of instantaneous u-velocities was computed. This process was repeated for a subset of 6,000 consecutive frames, from which four independent time signals were reconstructed. A power-spectral-density estimation was then computed for the four representative locations. The respective spectral plots are shown in Fig. 13 (b) - (e).

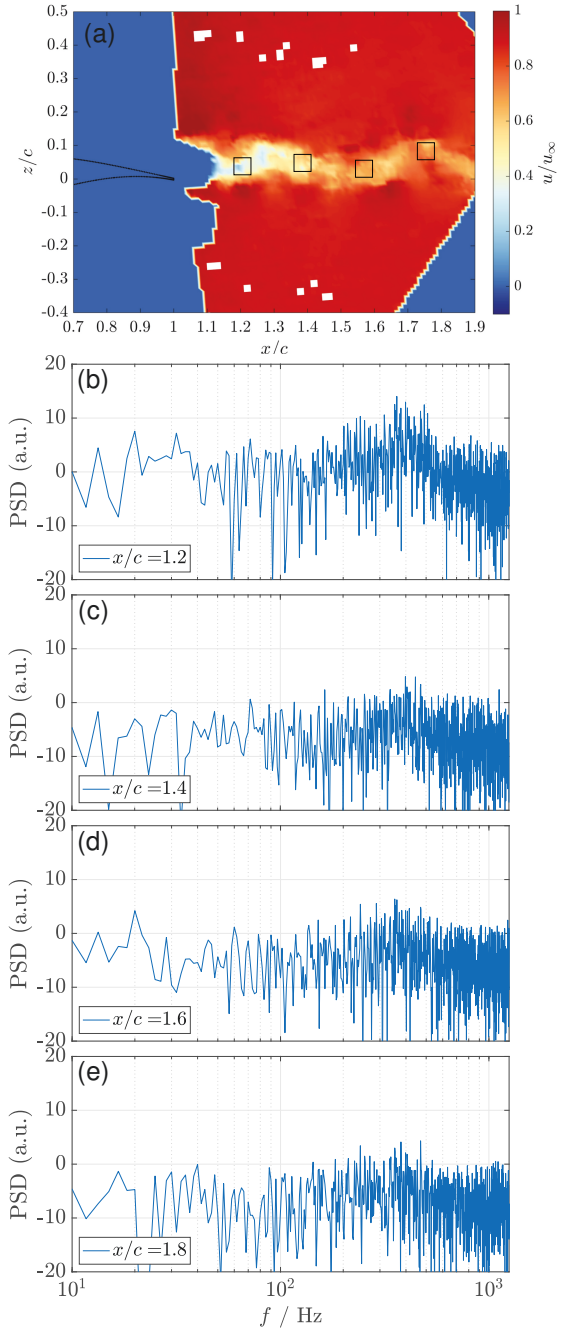

FIG 13. Power spectral density of streamwise velocity fluctuation at different location along the wake region (semi-logarithmic representation); airfoil not to scale

Enhanced spectral contributions associated with the fluctuating streamwise velocity component are discernible at all longitudinal stations between $f = 200$ Hz and $f = 600$ Hz.

However, the region immediately downstream of the trailing edge ($x/c = 1.2$) contains the most distinct narrow-band frequency bumps, with prominent primary contributions at $f = 350\,\mathrm{Hz}$ and $f = 480\,\mathrm{Hz}$ and secondary spikes at $f = 400\,\mathrm{Hz}$ and $f = 510\,\mathrm{Hz}$. Major contributions at the second location ($x/c = 1.4$) are $400\,\mathrm{Hz}$, $430\,\mathrm{Hz}$, and $460\,\mathrm{Hz}$; $360\,\mathrm{Hz}$, and $470\,\mathrm{Hz}$ at the third location ($x/c = 1.6$); and $380\,\mathrm{Hz}$, and $480\,\mathrm{Hz}$ at the most downstream position ($x/c = 1.8$).
Despite the reduced distinctness in the spectral footprint at the downstream locations, dominant fluctuations were consistently identified and independently confirmed between $350\,\mathrm{Hz}$, and $480\,\mathrm{Hz}$.
These finding agree nicely with the broadband spectral nature of the phenomenon 3D buffet reported in earlier studies [5,11]. The extracted values are equivalent to a dimensionless frequency of $St_{MAC} = 0.28$ to $St_{MAC} = 0.39$, expressed as the Strouhal number based on the mean aerodynamic chord (MAC). This is in good agreement with the range relevant to 3D buffet reported by Paladini et al. [18] and Giannelis et al. [11], and a value of $St_{MAC} = 0.30$ found experimentally by Koike et al. [17].

5. CONCLUSIONS

The velocity field past a 3D swept wing in transonic buffet conditions at a high, flight-realistic Reynolds number of $Re = 12.9 \cdot 10^6$ was assessed in detail for the first time. Stereoscopic planar CryoPIV measurements at two consecutive, partially overlapping fields of view gave access to all three velocity components across a large measurement region from $x/c = 0.3$ to $x/c = 1.9$. Phase-averaged representations of the velocity fields were presented to quantify the variation induced by the unsteady shock motion associated with the buffet condition. We demonstrated that due to a limited shock-buffet amplitude of about $0.05\,c$, the global variation of the flow topology is also limited. In this swept wing buffet case, there was no strict coupling between the up- and downstream motion of the shock wave and a large-scale modification of the global flow topology – in contrast with fully-established 2D airfoil buffet, where the flow topology is strongly modulated by the varying shape and strength of the shock wave. However, a pronounced streamwise velocity deficit was identified in the vicinity of the trailing edge, but it almost completely recovered within just one chord length downstream.
The vertical velocity map revealed a spatially confined downwash region starting slightly ahead of the trailing edge ($x/c = 0.8$). This downwash is gradually overcompensated by a dominant upwards deflection of the flow originating from the pressure side. The coalescence of the two flow fields from the suction and pressure sides results in a pure upwards motion beyond $x/c = 1.7$.
In addition, the complex organization of the spanwise velocity field modulated by the shock wave on the wing upper surface was demonstrated. A distinct spanwise contribution of constant magnitude in the wake to at least one chord length downstream of the trailing edge was observed.
Regarding the similarities and differences between 3D wing buffet and 2D airfoil buffet, we demonstrated the broadband nature of wing buffet on the basis of velocity fluctuations from PIV in the wake region. An analysis of high-speed PIV measurements in the wing wake field allowed to reconstruct the dominant frequencies associated with the transonic shock buffet phenomenon and showed that the spectral signature imposed by the unsteady shock motion continues to exist up until at least one chord length downstream of the trailing edge. Most probably, these influences will persist until much farther downstream, since they were not close to decaying at the end of our measurement window. Any aerodynamic devices impacted by the wake, such as the tailplane, would therefore be confronted with this buffet-induced spectral content of the partially asymmetric wake flow.

ACKNOWLEDGEMENTS

The authors gratefully acknowledge the German Research Foundation (Deutsche Forschungsgemeinschaft, DFG) for funding this work in the framework of the research unit FOR 2895 'Unsteady flow and interaction phenomena at high speed stall conditions' (project number 406435057). The authors would like to thank the Helmholtz Association of German Research Centres (HGF, Helmholtz-Gemeinschaft Deutscher Forschungszentren) and the German Aerospace Center (DLR, Deutsches Zentrum für Luft- und Raumfahrt) for financing the wind tunnel measurements. Further, the authors wish to thank Airbus for providing the XRF1 wind tunnel model and ETW for its work share in the framework of this project.

References

[1] J. B. McDevitt and A. F. Okuno. Static and dynamic pressure measurements on a naca 0012 airfoil in the ames high reynolds number facility. NASA Technical Paper 2485, June 1985.

[2] P. Molton, J. Dandois, A. Lepage, V. Brunet, and R. Bur. Control of buffet phenomenon on a transonic swept wing. AIAA Journal, 51(4):761–772, 2013. DOI: 10.2514/1.J051000.

[3] J. B. McDevitt, L. L. Levy, and G. S. Deiwert. Transonic flow about a thick circular-arc airfoil. AIAA Journal, 14(5):606–613, 1976. DOI: 10.2514/3.61402.

[4] L. Jacquin, P. Molton, S. Deck, B. Maury, and D. Soulevant. Experimental study of shock oscillation over a transonic supercritical profile. AIAA Journal, 47(9):1985–1994, 2009. DOI: 10.2514/1.30190.

[5] B. Benoit and I. Legrain. Buffeting prediction for transport aircraft applications based

on unsteady pressure measurements. AIAA 5th Applied Aerodynamics Conference, 1987. DOI: 10.2514/6.1987-2356.

[6] J. Crouch, A. Garbaruk, D. Magidov, and A. Travin. Origin and structure of transonic buffet on airfoils. 5th AIAA Theoretical Fluid Mechanics Conference, 2008. DOI: 10.2514/6.2008-4233.

[7] W. F. Hilton and R. G. Fowler. Photographs of shock wave movement. Aeronautical Research Council Reports and Memoranda, (2692), 1947.

[8] B. H. K. Lee. Oscillatory shock motion caused by transonic shock boundary-layer interaction. AIAA Journal, 28(5):942–944, 1990. DOI: 10.2514/3.25144.

[9] A. Hartmann, A. Feldhusen, and W. Schröder. On the interaction of shock waves and sound waves in transonic buffet flow. Physics of Fluids, 25(2), 2013. DOI: 10.1063/1.4791603.

[10] A. Feldhusen-Hoffmann, C. Lagemann, S. Loosen, P. Meysonnat, M. Klaas, and W. Schröder. Analysis of transonic buffet using dynamic mode decomposition. Experiments in Fluids, 62(4):66, 2021. DOI: 10.1007/s00348-020-03111-5.

[11] N. F. Giannelis, G. A. Vio, and O. Levinski. A review of recent developments in the understanding of transonic shock buffet. Progress in Aerospace Sciences, 92:39–84, 2017. DOI: https://doi.org/10.1016/j.paerosci.2017.05.004.

[12] F. Sartor, M. Minervino, J. Wild, S. Wallin, H. Maseland, J. Dandois, V. Georgievich Soudakov, and P. Vrchota. A cfd benchmark of active flow control for buffet prevention. CEAS Aeronautical Journal, 2019.

[13] L. Jacquin, V. Brion, P. Molton, D. Sipp, J. Dandois, S. Deck, F. Sartor, E. Coustols, and D. Caruana. Testing in aerodynamics research at onera: the example of the transonic buffet. AerospaceLab, 12, December 2016.

[14] J. D. Crouch, A. Garbaruk, and M. Strelets. Global instability in the onset of transonic-wing buffet. Journal of Fluid Mechanics, 881:3–22, oct 2019. DOI: 10.1017/jfm.2019.748.

[15] F. W. Roos. The buffeting pressure field of a high-aspect-ratio swept wing. 18th Fluid Dynamics and Plasmadynamics and Lasers Conference, 1985. DOI: 10.2514/6.1985-1609.

[16] C. V. Eckstrom, D. A. Seidel, and M. C. Sandford. Unsteady pressure and structural response measurements on an elasticsupercritical wing. Journal of Aircraft, 27(1):75–80, 1990. DOI: 10.2514/3.45898.

[17] S. Koike, M. Ueno, K. Nakakita, and A. Hashimoto. Unsteady pressure measurement of transonic buffet on nasa common research model. 34th AIAA Applied Aerodynamics Conference, 2016. DOI: 10.2514/6.2016-4044.

[18] E. Paladini, J. Dandois, D. Sipp, and J.-Ch. Robinet. Analysis and comparison of transonic buffet phenomenon over several three-dimensional wings. AIAA Journal, 57(1):379–396, 2019. DOI: 10.2514/1.J056473.

[19] P. C. Steimle, D.-C. Karhoff, and W. Schröder. Unsteady transonic flow over a transport-type swept wing. AIAA Journal, 50(2):399–415, 2012. DOI: 10.2514/1.J051187.

[20] F. Sartor, C. Mettot, and D. Sipp. Stability, receptivity, and sensitivity analyses of buffeting transonic flow over a profile. AIAA Journal, 53:1980–1993, 07 2015. DOI: 10.2514/1.J053588.

[21] J. Dandois. Experimental study of transonic buffet phenomenon on a 3d swept wing. Physics of Fluids, 28(1):016101, 2016. DOI: 10.1063/1.4937426.

[22] R. Konrath, R. Geisler, J. Agocs, D. Otter, H. Ehlers, F. Philipp, and J. Quest. Tracking the nacelle vortex above aircraft wing in the etw at real mach- and reynolds numbers by means of piv. 53rd AIAA Aerospace Sciences Meeting. DOI: 10.2514/6.2015-1560.

[23] R. Konrath, R. Geisler, J. Agocs, H. Ehlers, F. Philipp, and J. Quest. High-speed piv applied to wake of nasa crm model at high re-number sub- and transonic stall conditions. CEAS Aeronautical Journal, 9, 08 2017. DOI: 10.1007/s13272-017-0258-z.

[24] R. Geisler. A fast double shutter system for CCD image sensors. Measurement Science and Technology, 25(2):025404, jan 2014. DOI: 10.1088/0957-0233/25/2/025404.

[25] C. J. Schauerte and A.-M. Schreyer. Characterization of shock buffet on a supercritical 2d airfoil in transonic flow. 20th International Symposium on Application of Laser and Imaging Techniques to Fluid Mechanics, 2022.

[26] S. Timme and R. Thormann. Towards three-dimensional global stability analysis of transonic shock buffet. AIAA Atmospheric Flight Mechanics Conference, 2016. DOI: 10.2514/6.2016-3848.

[27] M. Iovnovich and D. E. Raveh. Numerical study of shock buffet on three-dimensional wings. AIAA Journal, 53(2):449–463, 2015. DOI: 10.2514/1.J053201.

[28] D. E. Raveh. Numerical study of an oscillating airfoil in transonic buffeting flows. AIAA Journal, 47(3):505–515, 2009. DOI: 10.2514/1.35237.